Scottish Universities Environmental Research Centre

Using optically stimulated luminescence to unravel sedimentary processes of the Usumacinta and Grijalva Rivers (SE Mexico)

Luminescence Laboratory Report

November 2012

T.C. Kinnaird[1], E. Muñoz-Salinas[2] and D.C.W. Sanderson[1]

[1]SUERC, East Kilbride, G75 OQF
[2] Instituto de Geología, Universidad Nacional Autónoma de México,
Circuito de la Investigación Científica, Ciudad Universitaria,
04510 México, D.F.

East Kilbride Glasgow G75 0QF Telephone: 01355 223332 Fax: 01355 229898

University of Glasgow

The University of Glasgow, charity number SC004401

The University of Edinburgh is a charitable body, registered in Scotland, with registration number SC005336

Summary

This report provides an optically stimulated luminescence (OSL) chronology for sediment collected through terrace deposits of the Usumacinta and Grijalva rivers in SE Mexico. The Grijalva and Usumacinta rivers are susceptible to flooding during the hurricane season (between May and November), affecting the population of the state of Tabasco, and leaving many households at a flood risk. The present study was initiated to obtain an understanding of the sediment processes, rates and frequency of flood events in the past.

The report summaries the initial luminescence profiling, using a SUERC PPSL system, and laboratory analysis, used to characterise the stratigraphy and interpret sedimentary processes in each profile, together with the quantitative quartz SAR dating used to define chronologies in each. Initial luminescence profiling revealed that the stratigraphy in each was complex, reflecting multiple cycles of deposition, with maxima, followed by a tail to lower intensities, possibly indicating deposition during extreme flood events, followed by a period in which the sediment was mixed and the luminescence signals reset. The laboratory profiling reproduced the apparent maxima/trends in the field profiling dataset. In the Grijalva section, the profiling samples encompass the full range of variations in the IRSL net signal intensities, re-affirming the complex stratigraphy. In the Usumacinta section, the profiling samples were positioned on the trend of a normal age-depth progression, which may indicate that the horizons sampled are well suited for quartz SAR dating.

Given the nature of the sediment sampled, it is unsurprising that the equivalent dose distributions obtained for each of the dating samples showed considerable scatter, leading to some ambiguity in estimating a stored dose for age calculations. In each, a number of aliquots returned high equivalent dose values, implying residual luminescence signals (leading to higher apparent ages), and others, low values, implying re-setting of the luminescence signals in the modern environment. It is well recognised that fluvial sediment of this sort can enclose mixed-age populations. It has been argued elsewhere (Fuchs and Lang, 2001; Lepper et al., 2000; Olley et al., 1998; Olley et al., 1999) that the lowest population of dose(s) may best represent the burial dose of the youngest depositional component, and that an arbitrary value of say the lowest 5% be used in age calculations. However, if this method was instigated for the Mexican samples, it would include the low equivalent dose values thought to reflect contamination from the surface, by bioturbation or some other weathering process, leading to artificially young ages. Therefore, each sample was evaluated on an individual basis, where low equivalent doses were considered to represent contamination and rejected, along with high equivalent dose outliers and any aliquots which failed SAR acceptance criteria. The weighted mean and weighted standard deviation of the reduced set were used in age calculations.

The dating results reported here provide a first chronology to interpret the changing fluvial dynamics of the Usumacinta and Grijalva rivers, and a means to quantify flood events through the historical period. The chronology established for the Grijalva section spans from the 6th century AD to the 12th century AD; and the chronology for the Usumacinta section from the 17th century AD to the 19th century AD.

Contents

List of Figures

List of Tables

1. Introduction

This report is concerned with optically stimulated luminescence (OSL) investigations of sediment collected from two sediment stratigraphies in SE Mexico, from sections on the Grijalva and Usumacinta rivers.

The Usumacinta River is formed from the confluence of the Pasión and Salinas rivers, arising in the Sierra de Santa Cruz and Sierra Madre de Guatemala, respectively. The river defines part of the border between Mexico and Guatemala. It enters Mexican territory, approximately 10 km south of Tenosique, and meanders through the state of Tsabasco to the Gulf of Mexico, where it discharges to the Bay of Campeche (Fig. 1-1). It has a length of some ~ 1,900 km. The Grijalva River has its headwaters in the Chiapas highlands, and flows from Chiapas, through the state of Tabasco, into the Bay of Campeche. The river has a length of 480 km, and its drainage basin is 134,400 km^2.

The Grijalva and Usumacinta rivers converge at Tres Brazos, Centla, forming a large floodplain, the plain of Tabasco. This floodplain is susceptible to flooding during the hurricane season (between May and November). The present study was initiated to obtain an understanding of the sediment processes, rates and frequency of flood events for the Grijalva and Usumacinta rivers through history. This report concerns the OSL dating of sediment from two stratigraphies along the Grijalva and Usumacinta rivers to provide a chronological framework to interpret sedimentary processes and rates.

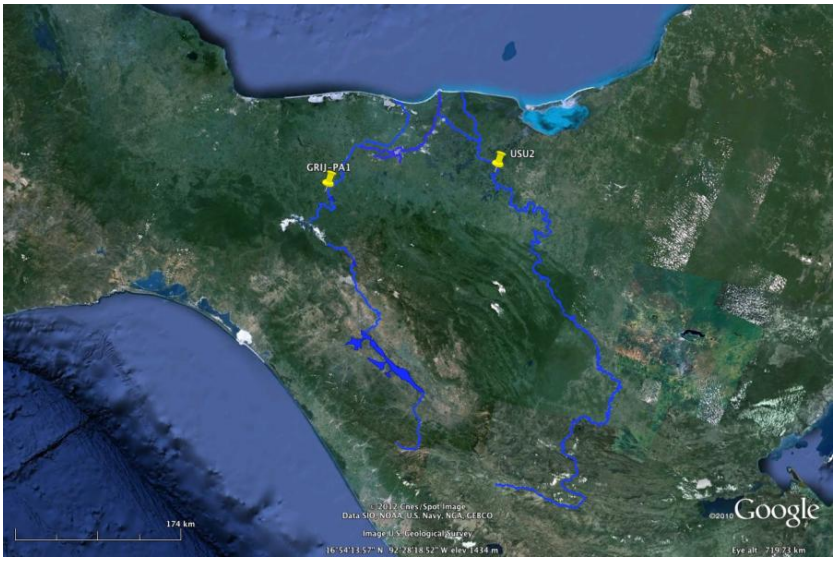

Figure 1-1: Location map: The course/trace of the two rivers, Grijalva (left) and Usumacinta (right) are shown; together with the location of the two sections sampled

2. Sampling

Sampling was undertaken by Esperanza Muñoz-Salinas during the summer of 2012. Photographs of the two sediment stratigraphies are reproduced in figures 1-1 and 1-2.

Figure 2-1: Section GRIJ.PA1, Grijalva River

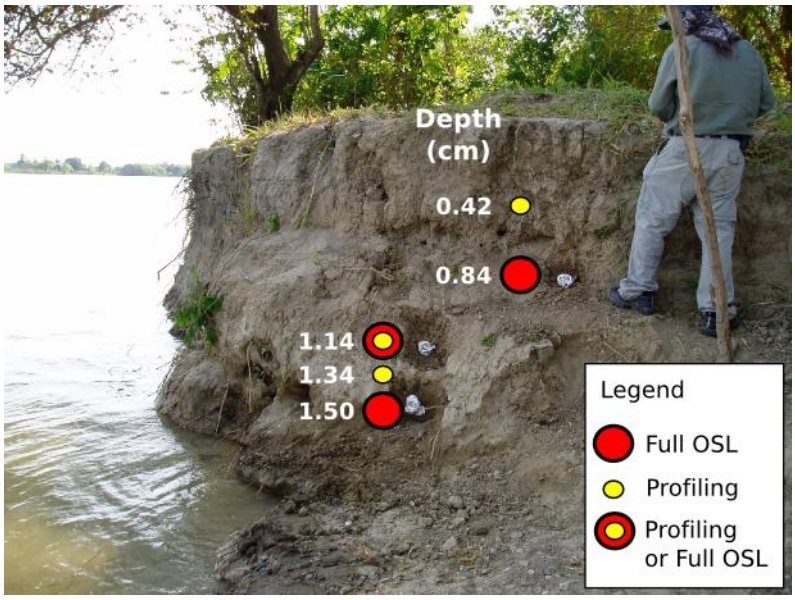

Figure 2-2: Section USU2, Usumacinta River

Samples were submitted to the luminescence laboratories at the Scottish Universities Environmental Research Centre (SUERC) for dating in July 2012. Sample numbers, contexts, and unique laboratory code (assigned on receipt) are listed in Table 2-1.

	SUTL no.	
Sample depth	Profiling	Full Quartz SAR
Grijalva River		
0.18	SUTL2510A	
0.49		SUTL2508
0.88	SUTL2510B	
1.18	SUTL2510C	
1.36		SUTL2509

Usumacinta River		
0.42	SUTL2514A	
0.84		SUTL2511
1.14	SUTL2514B	SUTL2512
1.34	SUTL2514C	
1.50		SUTL2513

Table 2-1: SUTL sample reference numbers

During fieldwork, Esperanza Muñoz-Salinas made use of a SUERC PPSL system to explore IRSL net signal variations within each profile, in a similar manner to that described by Sanderson and Murphy (2010) using the SUERC portable OSL reader, to characterise the stratigraphy in each, and identify sedimentary phases and potential horizons for dating (Fig. 2-3).

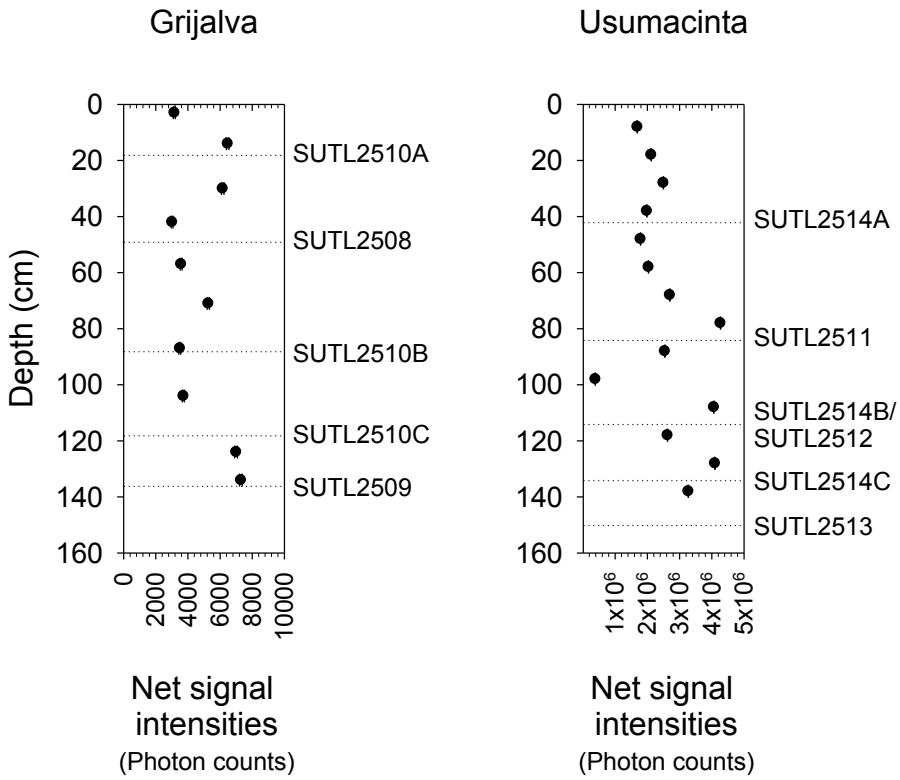

Figure 2-3: Net IRSL signal intensities obtained for profiling samples taken at ~10 cm spacing through the two sediment stratigraphies

In each profile there is a large spread in net signal intensities with depth suggesting that the stratigraphy in each is complex, with variable zeroing of the sediment on deposition. Interestingly though, there is a broad increase in luminescence signals with depth, implying that overall, there is a normal age-depth progression through each profile. Notably, net IRSL signal intensities are two orders of magnitude larger in the Usumacinta profile than they are in the Grijalva profile. It is interesting to speculate on why this may be so: if one assumes that the sediment in each profile has similar mineralogy, mineral characteristics, radionuclide concentrations etc, then this

may indicate that sediment within the Usumacinta profile is older? The laboratory analysis will provide a further insight into the variation in luminescence signals.

The positions of the profiling and full dating samples are shown, relative to the field profiling dataset, for the Grijalva and Usmacinta sections, in figure 2-3. In the Grijalva section the sample locations encompass the full range of variations in IRSL net signal intensities, including the maxima at 14 - 30 cm depth, 71 cm and the tail to higher values after 124 cm. It will be interestingly to see if the variations in IRSL net signal intensities correspond to variations in luminescence sensitivities and stored dose values through the profile. It is worth noting that the amalgamation of the laboratory profiling and full dating datasets may not produce a normal age-depth progression, as the profiling samples are located at maxima in the field profiling dataset, and the full dating samples are located on the part of the profile that shows a normal age progression. In contrast, the sample locations through the Usumacinta profile were taken from horizons which show a normal progression in luminescence signals with depth, avoiding the maxima or spikes in the field profiling dataset. So whereas the sample positions through the Grijalva profile encompass the complex stratigraphy, the sample positions through the Usumacinta profile may potentially mask the complex stratigraphy.

3. Calibrated laboratory luminescence screening measurements

3.1. Methodology

All sample handling and preparation was conducted under safelight conditions in the SUERC luminescence dating laboratories. The profiling samples were wet sieved to extract the 90-250 μm fractions, which were then treated with 1M HCl for 10 minutes. The samples were split into two fractions, one for polymineral analysis and one for quartz analysis. The quartz subsample was treated with 40% HF for 40 minutes, to dissolve the less chemically resistant minerals and to etch the outer part of the grains. The HF etched material was then treated with 1 M HCl for 10 minutes to dissolve any precipitated fluorides. The grains were presented for measurement on 10 mm in diameter stainless steel discs.

Luminescence sensitivities (Photon Counts per Gy) and stored doses (Gy) were evaluated from paired aliquots of the HF-etched quartz and polymineral fractions, using Risø DA-15 automatic readers. The readout cycles comprised a natural readout, followed by readout cycles for a nominal 1Gy test dose, a 5Gy regenerative dose, and a further 1Gy test dose. For the quartz samples, a 240˚C preheat was used with 60s OSL measurements using the blue LEDs. For the polymineral samples, a 260˚C preheat was followed by 60s OSL measurements using the IR LEDs at 50˚C, the IR LEDs at 225˚C (the post-IR IRSL signal), the blue LEDs at 125˚C, and a TL measurement to 500˚C.

3.2. Results

The data are presented graphically in figures 4-1 and 4-2, for the two profiles respectively. The data is tabulated in Appendix A.

In the Grijalva profile, the laboratory profiling dataset reproduces the apparent maxima trends in the field profiling set, reflecting the sections complex stratigraphy. The maxima noted in the field profiling dataset for strata between 14 - 30 cm depth is reproduced in the laboratory profiling dataset (i.e. at 18 cm depth), as is the maxima noted between 57 - 87 cm depth. Interestingly, the stored dose values obtained for strata at the base of the sequence are lower than those obtained at height. This raises several questions: (i) are the differences in stored dose estimates between the top and bottom of the profile controlled by variations in the environmental dose rate, such that the units are similar in age? or, (ii) that the stored dose values obtained for strata at the base of the profile represent the true age of the accumulation, and that the overlying strata, with the higher stored dose values, represent accumulations that where poorly reset on deposition? Full dose rate determinations will be made at each of the full dating sample positions, and provide a means to test these two hypotheses. It is notable that the quartz OSL stored doses are much lower than those obtained from polymineral IRSL and OSL, which are in turn lower than polymineral TL. The data raise questions as to whether the larger IRSL, OSL and TL signals in the polymineral phase represent poor bleaching on deposition? and whether the higher stored dose values in the polymineral phase represent signal inheritance?

Interestingly, the stored dose values obtained for the Usumacinta section are lower than those obtained for Grijalva. The variations in IRSL net signal intensities noted between profiles (in the field profiling dataset) are therefore controlled by mineral behaviour (i.e. luminescence sensitivities), and not age. The emerging picture for the Usumacinta profile is that the stratigraphy in this section is slightly less complex. Quartz OSL signals, and polymineral OSL, IRSL and TL signals, increase with depth, implying a normal age-depth progression. Given the large variations in net signal intensities within the field profiling dataset, it may be that the positioning of the laboratory profiling and full dating samples has been more fortuitous, in that the horizons with large variations are not sampled.

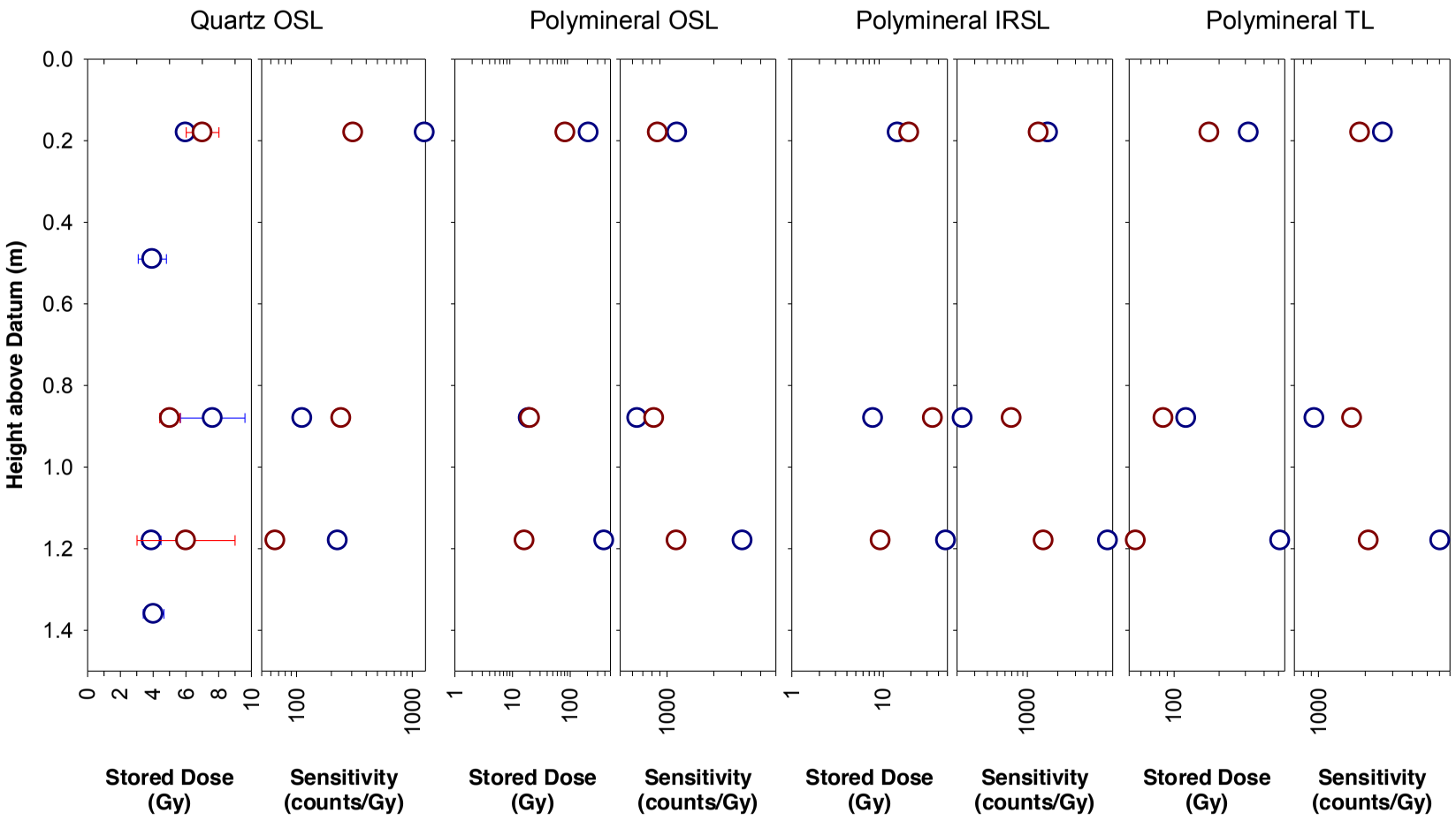

Figure 3-1: Laboratory profiling results, Grijalva River (Section GRIJ.PA1)

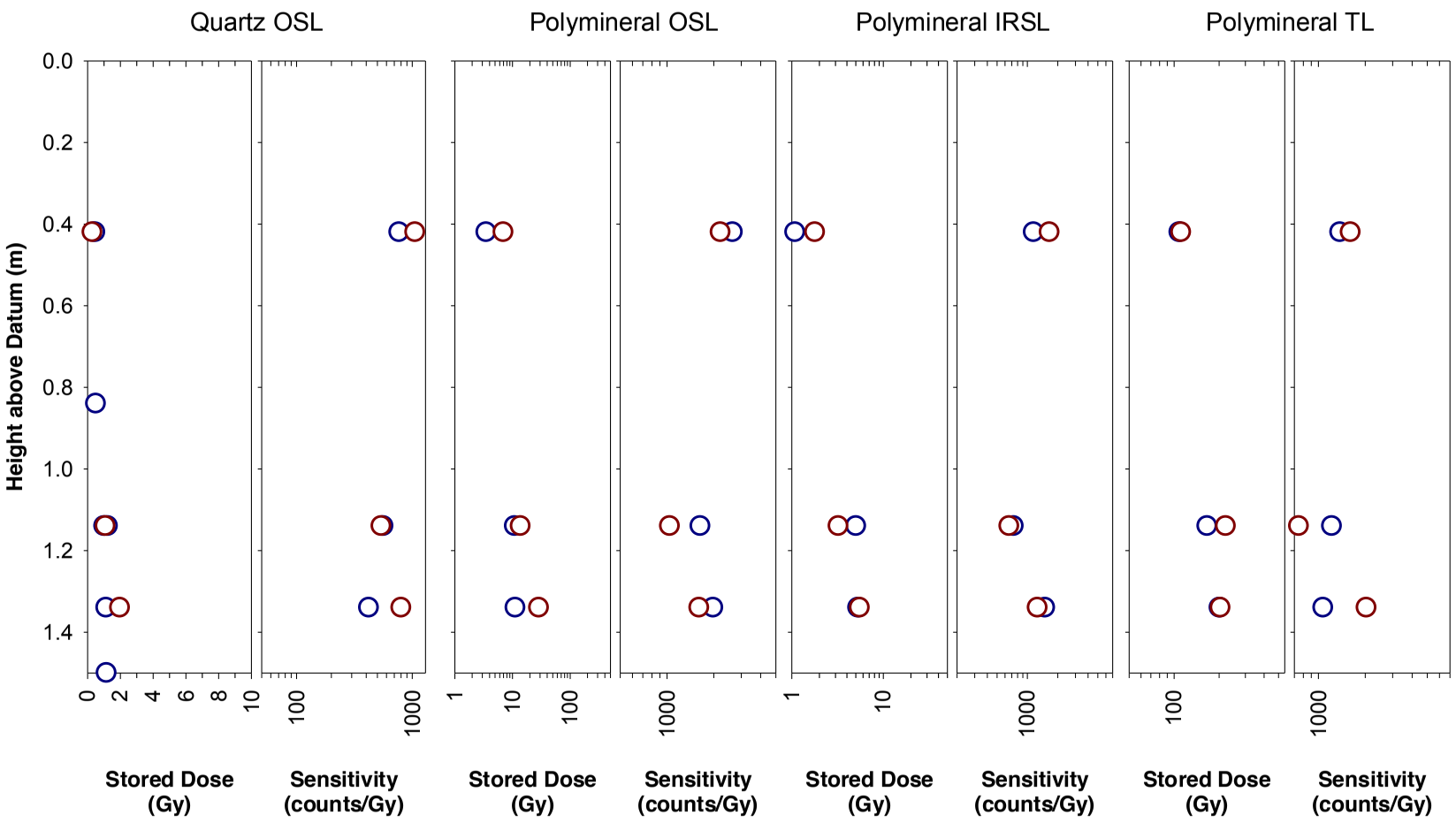

Figure 3-2: Laboratory profiling results, Usumacinta River (Section USU2)

4. Quartz SAR measurements

4.1. Sample preparation

All sample handling and preparation was conducted under safelight conditions in the SUERC luminescence dating laboratories.

4.1.1. Water contents

Bulk samples were weighed, saturated with water and re-weighed. Following oven drying at 50 °C to constant weight, the actual and saturated water contents were determined as fractions of dry weight. These data were used, together with information on field conditions to determine water contents and an associated water content uncertainty for use in dose rate determination.

4.1.2. HRGS and TSBC Sample Preparation

Bulk quantities of material, weighing c. 100-125 g, were removed from each full dating sample for environmental dose rate determinations. This material was placed in an oven to dry to constant weight. Approximately 100 g of dried material from each sample was weighed into a HDPE pot for a high-resolution gamma spectrometry (HRGS) measurement. From each of these samples, 20 g of material was temporary removed and used in thick source beta counting (TSBC; Sanderson, 1988). This material was then returned to the relevant pot, sealed with epoxy resin and left for 3 weeks prior to measurement to allow equilibration of ^{222}Rn daughters.

4.1.3. SAR Sample Preparation

Approximately 20g of material was removed for each tube and processed for luminescence measurements, to separate sand-sized quartz and feldspar grains. The sample was wet sieved to obtain the 90-150 and 150-250 μm fractions. The 150-250 μm sub-sample was treated with 1 M hydrochloric acid (HCl) for 10 minutes, 15% hydrofluoric acid (HF) for 15 minutes, and 1 M HCl for a further 10 minutes. This etched material was then centrifuged in sodium polytungstate solutions of ~2.51, 2.58, 2.62, and 2.74 gcm^{-3}, to obtain concentrates of potassium-rich feldspars (2.51-2.58 gcm^{-3}), sodium feldspars (2.58-2.62 gcm^{-}3) and quartz plus plagioclase (2.62-2.74 gcm^{-3}). The selected quartz fraction was then subjected to further HF and HCl washes (40% HF for 40mins, followed by 1M HCl for 10 mins). All materials were dried at 50°C and transferred to Eppendorf tubes. 16 aliquots were produced for each sample.

4.2. Measurements and determinations

4.2.1. Dose rate determinations

Dose rates were measured in the laboratory using HRGS and TSBC. Full sets of dose rate determinations were made for samples SUTL2508 to SUTL2509, and SUTL2511 to SUTL2513.

HRGS measurements were performed using a 50% relative efficiency "n" type hyper-pure Ge detector (EG&G Ortec Gamma-X) operated in a low background lead shield with a copper liner. Gamma ray spectra were recorded over the 30 keV to 3 MeV range from each sample, interleaved with background measurements and measurements from SUERC Shap Granite standard in the same geometries. Counting times of 80ks per sample were used. The spectra were analysed to determine count rates from the major line emissions from ^{40}K (1461 keV), and from selected nuclides in the U decay series (^{234}Th, ^{226}Ra + ^{235}U, ^{214}Pb, ^{214}Bi and ^{210}Pb) and the Th decay series (^{228}Ac, ^{212}Pb, ^{208}Tl) and their statistical counting uncertainties. Net rates and activity concentrations for each of these nuclides were determined relative to Shap Granite by weighted combination of the individual lines for each nuclide. The internal consistency of nuclide specific estimates for U and Th decay series nuclides was assessed relative to measurement precision, and weighted combinations used to estimate mean activity concentrations (Bq kg^{-1}) and elemental concentrations (% K and ppm U, Th) for the parent activity. These data were used to determine infinite matrix dose rates for alpha, beta and gamma radiation.

Beta dose rates were also measured directly using the SUERC TSBC system (Sanderson, 1988). Sample count rates were determined with six replicate 600 s counts for each sample, bracketed by background measurements and sensitivity determinations using the Shap Granite secondary reference material. Infinite-matrix dose rates were calculated by scaling the net count rates of samples and reference material to the working beta dose rate of the Shap Granite (6.25 ± 0.03 mGy a^{-1}). The estimated errors combine counting statistics, observed variance and the uncertainty on the reference value.

The dose rate measurements were used in combination with the assumed burial water contents, to determine the overall effective dose rates for age estimation. Cosmic dose rates were evaluated by combining latitude and altitude specific dose rates (0.181 ± 0.01 mGy a^{-1}) for the site with corrections for estimated depth of overburden using the method of Prescott and Hutton (1994).

4.2.2. SAR luminescence measurements

All measurements were conducted using a Risø DA-15 automatic reader equipped with a ^{90}Sr/^{90}Y β-source for irradiation, blue LEDs emitting around 470 nm and infrared (laser) diodes emitting around 830 nm for optical stimulation, and a U340 detection filter pack to detect in the region 270-380 nm, while cutting out stimulating light (Bøtter-Jensen et al., 2000). For each sample, equivalent dose determinations were made on sets of 16 aliquots per sample, using a single aliquot regeneration (SAR) sequence (cf Murray and Wintle, 2000). According to this procedure, the OSL signal level from an individual disc is calibrated to provide an absorbed dose estimate (the equivalent dose) using an interpolated dose-response curve, constructed by regenerating OSL signals by beta irradiation in the laboratory. Sensitivity changes which may occur as a result of readout, irradiation and preheating (to remove unstable radiation-induced signals) are monitored using small test doses after each regenerative dose. Each measurement is standardised to the test dose response determined immediately after its readout, to compensate for observed changes in sensitivity during the laboratory measurement sequence. For the purposes

of interpolation, the regenerative doses are chosen to encompass the likely value of the equivalent (natural) dose (determined in the initial laboratory characterisation study, see section 4). A repeat dose point is included to check the ability of the SAR procedure to correct for laboratory-induced sensitivity changes (the 'recycling test'; table 5-1), a zero dose point is included late in the sequence to check for thermally induced charge transfer during the irradiation and preheating cycle (the 'zero cycle'; table 5-1), and an IR response check is included to assess the magnitude of non-quartz signals. Regenerative dose response curves were constructed using doses of 1, 5, 10 and 30 Gy, with a test dose of 2 Gy (Table 5-1).

Aliquot	Operation	Cycle:	1	2	3	4	5	6	7	8
		Details	Natural					Zero	Recycling	IR Response
1-20	Regenerative Dose	"X" Gy $^{90}Sr/^{90}Y$	no	1	5	10	30	0	5	5
1-5	Preheat	200°C for 30s	yes	yes	yes	yes	yes	yes	yes	yes
6-10	Preheat	220°C for 30s	yes	yes	yes	yes	yes	yes	yes	yes
11-15	Preheat	240°C for 30s	yes	yes	yes	yes	yes	yes	yes	yes
16-20	Preheat	260°C for 30s	yes	yes	yes	yes	yes	yes	yes	yes
1-20	Measurement	OSL 60s at 125°C	yes	yes	yes	yes	yes	yes	yes	yes
1-20	Measurement	IRSL 60s at 50°C	no	no	no	no	no	no	no	yes
1-20	Test Dose (Td)	"X" Gy $^{90}Sr/^{90}Y$	2	2	2	2	2	2	2	2
1-5	Td Preheat	200°C for 30s	yes	yes	yes	yes	yes	yes	yes	yes
6-10	Td Preheat	220°C for 30s	yes	yes	yes	yes	yes	yes	yes	yes
11-15	Td Preheat	240°C for 30s	yes	yes	yes	yes	yes	yes	yes	yes
16-20	Td Preheat	260°C for 30s	yes	yes	yes	yes	yes	yes	yes	yes
1-20	Test Measurement	OSL 60s at 125°C	yes	yes	yes	yes	yes	yes	yes	yes

Table 4-1: Quartz Single Aliquot Regenerative (SAR) Sequence (Discs 1 -16)

4.3. Results

4.3.1. Dose rates

HRGS results are shown in Table 4-1, both as activity concentrations (i.e. disintegrations per second per kilogram) and as equivalent parent element concentrations (in % and ppm), based in the case of U and Th on combining nuclide specific data assuming decay series equilibrium. K, U and Th concentrations ranged between 1.8 and 2.5 %, 1.0 and 5.4 ppm and 3.0 to 10.9 ppm, respectively. Infinite matrix alpha, beta and gamma dose rates from HRGS are listed for all samples in Table 4-2, together with infinite matrix beta dose rates from TSBC. Gamma dose rates, as measured on dry samples in the laboratory, ranged between 0.88 ± 0.02 to 1.70 ± 0.04 mGy a^{-1}, with a mean value of 1.25 ± 0.32 mGy a^{-1}. Beta dose rates measured by HRGS ranged between 2.21 ± 0.07 to 2.89 ± 0.06 mGy a^{-1}, with a mean value of 2.42 ± 0.27 mGy a^{-1}. TSBC beta dose rate estimates ranged between 2.18 ± 0.06 to 2.62 ± 0.07 mGy a^{-1}, with a mean value of 2.35 ± 0.18 mGy a^{-1}. It is noted that there is a good agreement between the beta dose rates determined by HRGS and TSBC.

It is notable that there are variations in the radionuclide concentrations between sites: the Grijalva and Usumincinta rivers have catchments underlain by different geological units. The Grijalva river drains the 'Los Altos de Chiapas', a massif formed from felsic rocks (granites and rhyolites) in its upper part, and limestones in its lowest parts. The Usmacinta river arises in Guatemala, and largely bypasses the massif, in its lower reaches, its catchment is underlain by limestones. It is possible that the radionuclide signatures in both sections reflect their proximity to the massif, and/or the geology in their lower reaches: the K enrichment in the Grijalva profile may reflect its proximity to the felsic core of the massif; and the relative U and Th enrichment in the Usmacinta profile, may reflect the fact that this river preferentially samples from limestones in its lower reaches.

SUTL no.	Activity Concentration (Bq kg^{-1})[a]			Equivalent Concentration[b]		
	^{40}K	U	Th	K (%)	U (ppm)	Th (ppm)
2508	664 ± 22	23 ± 3	22 ± 2	2.15 ± 0.07	1.85 ± 0.22	5.41 ± 0.42
2509	775 ± 18	12 ± 1	13 ± 1	2.50 ± 0.06	1.00 ± 0.10	3.13 ± 0.19
2511	668 ± 15	67 ± 4	44 ± 1	2.16 ± 0.05	5.39 ± 0.32	10.96 ± 0.27
2512	566 ± 14	51 ± 3	34 ± 1	1.83 ± 0.04	4.16 ± 0.26	8.44 ± 0.24
2513	558 ± 14	49 ± 3	33 ± 1	1.80 ± 0.05	4.00 ± 0.24	8.23 ± 0.24

Table 4-2: Activity and equivalent concentrations of K, U and Th determined by HRGS

[a]Shap granite reference, working values determined by David Sanderson in 1986, based on HRGS relative to CANMET and NBL standards.

[b]Activity and equivalent concentrations for U, Th and K determined by HRGS (Conversion factors based on NEA (2000) decay constants): 40K: 309.3 Bq kg^{-1} $\%K^{-1}$, 238U: 12.35 Bq kg^{-1} $ppmU^{-1}$, 232Th: 4.057 Bq kg^{-1} ppm Th^{-1}.

SUTL no.	HRGS, dry (mGy a^{-1})[a]			TSBC, dry (mGy a^{-1})
	Alpha	Beta	Gamma	
2508	9.13 ± 0.68	2.21 ± 0.07	1.01 ± 0.04	2.41 ± 0.06
2509	5.09 ± 0.31	2.31 ± 0.05	0.88 ± 0.02	2.38 ± 0.06
2511	23.07 ± 0.92	2.89 ± 0.06	1.70 ± 0.04	2.62 ± 0.07
2512	17.78 ± 0.75	2.37 ± 0.05	1.35 ± 0.03	2.19 ± 0.06
2513	17.2 ± 0.69	2.32 ± 0.05	1.32 ± 0.03	2.18 ± 0.06

Table 4-3: Infinite matrix dose rates determined by HRGS and TSBC.
[a]based on dose rate conversion factors in Aikten (1983)

The water content measurements with assumed values for the average water content during burial are given in Table 4-3. The table also lists the gamma dose rate from the HRGS after application of a water content correction. Effective dose rates to the HF etched 200 μm quartz grains are given for the gamma dose rate and beta dose rate (the mean of the TSBC and HRGS data, accounting for water content and grain size).

SUTL No.	Water Content (%)			Effective Dose Rate (mGy a^{-1})		
	Fractional	Saturated	Assumed	Beta[a]	Gamma	Total[b]
2508	17.4	34.8	20 ± 5	1.68 ± 0.11	0.83 ± 0.02	2.69 ± 0.11
2509	16.4	19.3	20 ± 5	1.73 ± 0.10	0.72 ± 0.01	2.63 ± 0.11
2511	20.5	31.8	20 ± 5	2.03 ± 0.09	1.43 ± 0.02	3.65 ± 0.09
2512	22.1	35.5	25 ± 5	1.68 ± 0.08	1.14 ± 0.01	3.00 ± 0.08
2513	29.3	32.5	30 ± 5	1.66 ± 0.08	1.11 ± 0.01	2.95 ± 0.08

Table 4-4: Water contents, and effective beta and gamma dose rates following water correction.
[a] Effective beta dose rate combining water content corrections with inverse grain size attenuation factors obtained by weighting the 200 μm attenuation factors of Mejdahl (1979) for K, U, and Th by the relative beta dose contributions for each source determined by Gamma Spectrometry.

4.3.2. Single aliquot equivalent dose determinations

For equivalent dose determination, data from single aliquot regenerative dose measurements were analysed using the Risø TL/OSL Viewer programme to export integrated summary files that were analysed in MS Excel and SigmaPlot. Composite dose response curves were constructed from selected discs and for each of the four preheating groups from each sample, and used to estimate equivalent dose values for each individual disc and their combined sets. Dose response curves for each of the four preheating temperature groups and the combined data were determined using a fit to exponential function (Appendix B). The equivalent dose was then determined for each aliquot using the corresponding exponential fit parameters.

The distribution in equivalent dose values was examined using radial plotting methods (Appendix C). All samples revealed some heterogeneity in their equivalent dose distributions. To check for the presence of non-uniformity (sample heterogeneity) in sample radiation dose histories we compared aliquot intensity and equivalent doses. In figure 4-1 the mean, median, robust mean and the logged and

non-logged central age modelled mean of Galbraith (1999) are shown. The robust mean was calculated by two methods; by the use of an in-house excel program, which removed any data outwith 2 standard deviations in a continuous loop, so that data excluded from the last calculation was not included in the next; and by an excel add-in 'robust statistics' available from the Chemistry Society of London, which calculates a robust mean using Huber's estimate 2. In addition, the figure illustrates the large spread in estimated equivalent dose calculated using all six methods, implying that caution must be used in determining the equivalent dose to use in age calculations (see below).

Single aliquots were rejected from further analysis based on the test dose sensitivity check, SAR criteria checks, the robust mean, feldspar contamination and radial plots. Table 4-4 summarises the quality evaluation checks on the SAR data (once filtered); the mean sensitivity of each aliquot and sensitivity change, the recycling ratio and zero dose response.

SUTL No.	Mass (mg)	Sensitivity (counts/Gy)	Sensitivity change (%)	Recycling Ratio	Zero Dose (Gy)	IRSL response (%)
2508	1.52	622 ± 73	2.33 ± 0.4	0.98 ± 0.03	0.15 ± 0.05	1.12 ± 0.6
2509	2.03	10279 ± 3175	-2.31 ± 0.7	1.00 ± 0.01	-0.01 ± 0.14	22.45 ± 2.8
2511	1.14	1111 ± 130	1.11 ± 0.3	1.00 ± 0.02	0.17 ± 0.02	13.08 ± 3.9
2512	0.76	735 ± 217	1.29 ± 0.5	0.99 ± 0.02	0.09 ± 0.04	2.42 ± 0.7
2513	1.65	817 ± 221	0.30 ± 0.1	1.00 ± 0.01	0.05 ± 0.03	1.16 ± 0.4

Table 4-5: SAR quality parameters. Standard errors given.

In each sample, the heterogeneity in equivalent dose values reflects the nature of the sediment studied. It is well recognised that fluvial sediments have the potential for enclosing mixed-age luminescence populations, reflecting variable bleaching at deposition (i.e. a response to the filtering and attenuation of the solar spectrum in water, e.g. Sanderson et al., 2007). Each of the samples collected from terrace deposits of the Grijalva and Usmacinta rivers showed considerable scatter in there equivalent dose distributions, reflecting the fact that the sediment contains quartz grains that were well-bleached at deposition, and that others under a cover of water were incompletely bleached. In each, a number of aliquots may return low values, implying re-setting of the luminescence signals in the modern environment, whilst other aliquots tail to higher stored dose values. It is presumed that the low equivalent dose values reflect contamination from the surface, by bioturbation or some other process, as otherwise they would imply very young (modern) ages for the terraces. This is unsurprising, given that the terrace deposits lining the Grijalva and Usmacinta rivers were presumably deposited during flood events, when the rivers would have been turbid, and contained a high suspended sediment load.

For each sample, aliquots thought to represent contamination by bioturbation or other weathering process, and aliquots through to contain large residuals were rejected. Then, for each sample, the weighted mean and the weighted standard deviation were used to estimate the stored dose to be used in age determination; this mean value, hopefully, best represents the well-bleached component.

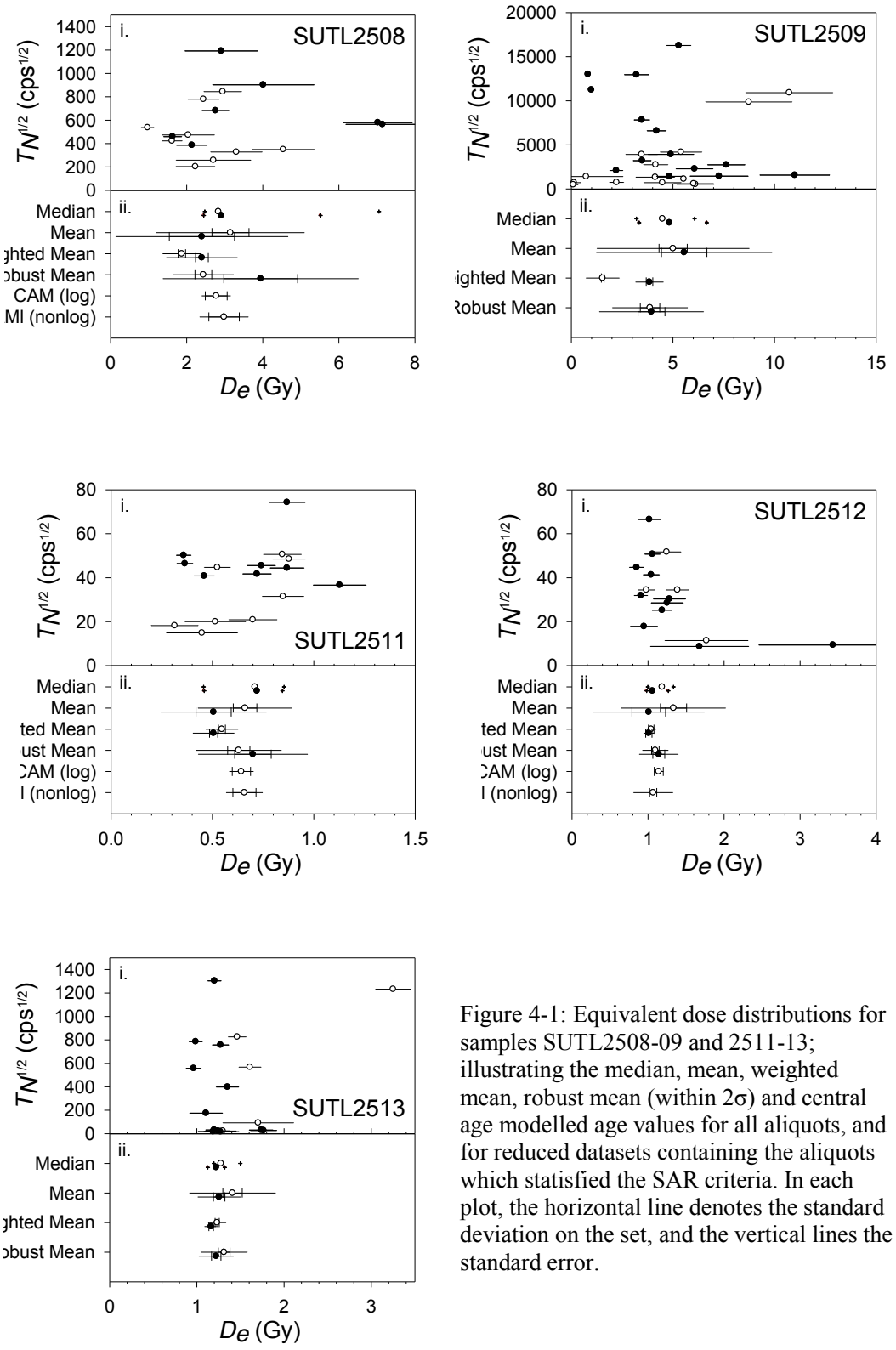

Figure 4-1: Equivalent dose distributions for samples SUTL2508-09 and 2511-13; illustrating the median, mean, weighted mean, robust mean (within 2σ) and central age modelled age values for all aliquots, and for reduced datasets containing the aliquots which statisfied the SAR criteria. In each plot, the horizontal line denotes the standard deviation on the set, and the vertical lines the standard error.

It has argued elsewhere (Fuchs and Lang, 2001; Lepper et al., 2000; Olley et al., 1998; Olley et al., 1999) that with fluvial sediments the best estimate of the true burial dose is the lowest measured dose, or population of dose(s), in these works the authors chose an arbitrary value to define the lowest population of doses, such as the lowest 5%. If this method was instigated for the Grijalva and Usmacinta samples, it would include the low equivalent dose values thought to reflect contamination from the surface, leading to artificially young ages.

4.3.3. Age determinations

The total dose rate is determined from the sum of the equivalent beta and gamma dose rates, and the cosmic dose rate. Age estimates are determined by dividing the equivalent stored dose by the dose rate. Uncertainty on the age estimates is given by combination of the uncertainty on the dose rates and stored doses, with an additional 5% external error. Table 4-6 lists the total dose rate, stored dose and corresponding age of the sample.

SUTL No.	Section	Depth	Dose Rate (mGy a^{-1})	Stored Dose (Gy)	Years BP	Calendar years
2508	Grijalva	0.49	2.69 ± 0.11	2.40 ± 0.94	0.89 ± 0.35	1120 ± 350
2509		1.36	2.63 ± 0.11	3.85 ± 0.68	1.47 ± 0.27	550 ± 270
2511	Usumacinta	0.84	3.65 ± 0.09	0.51 ± 0.10	0.14 ± 0.03	1870 ± 30
2512		1.14	3.00 ± 0.08	1.01 ± 0.07	0.34 ± 0.02	1670 ± 30
2513		1.50	2.95 ± 0.08	1.16 ± 0.08	0.39 ± 0.03	1620 ± 30

Table 4-6: OSL age determinations for samples SUTL2508-09 and 2511-13

Apparent ages were determined for each of the profiling samples. For the profiling samples that were positioned between full dating locations, the total dose rate was estimated by interpolation between the tube locations. For profiling samples positioned above full dating locations the total dose rate was estimated by extrapolating the dose rate trend through the lower positions. Equivalent dose determinations were scaled to the 5 Gy regenerative dose. Apparent age estimates were then calculated by combining the linear extrapolated dose estimate with the dose rates estimated for each position. It should be noted that this method will slightly underestimate the apparent dose for each of the profiling positions, as the composite dose response curves generated for the full dating samples are known to grow exponentially with regeneration dose.

5. Discussions and conclusions

Five sediment samples collected from terrace deposits of the Grijalva and Usumacinta rivers in SE Mexico were analysed by the quartz SAR method. It is well recognised that fluvial sediments of this sort have the potential for enclosing mixed-age populations, and indeed all of the samples show considerable scatter in their equivalent dose distributions, reflecting poor bleaching at the time of deposition and/or mixing of poorly bleached and unbleached material.

Nevertheless, through statistical analysis, dating results were obtained for both sections that are internally consistent, and provide a chronology to interpret the changing fluvial dynamics in each river, and a valuable tool to observe flood events through the historical period. The chronology established for the Grijalva section spans from the 6th century AD to the 12th century AD; and the chronology for the Usumacinta section from the 17th century AD to the 19th century AD.

One may augment the quartz SAR chronology with the apparent ages determined from each of the profiling positions. Rather than refining the chronology in each profile, the integrated dataset illustrates the complex stratigraphy preserved in each, and the variable bleaching received by the sediment. Of the two, the apparent chronology through the Usumacinta stratigraphy, appears to be a normal age-depth progression, and an attempt was made to determine sedimentation rates through this deposit (Table 5-1). It must be noted though that the field profiling dataset reveals that the stratigraphy elsewhere in this section is very complex, and that the sampling positions within this profile have been drawn from positions which do not cover the full range of signal variations observed in the PPSL profile. It is possible that further information on recent processes in these rivers could be gathered if more detailed sampling was undertaken,

SUTL no.	Depth (cm)	Stored dose (Gy)	Dose Rate (mGy a^{-1})	Calendar years (AD)	Δage (years)	Δdepth (mm)	Sed. rate (mm/yr)
River Grijalva							
2510A	0.18	6.51 ± 0.52	2.71 ± 0.16	390 ± 240	430	870	2.0 ± 0.1
2508	0.49	2.40 ± 0.94	2.69 ± 0.11	1120 ± 350	-	-	-
2510B	0.88	6.33 ± 1.31	2.66 ± 0.16	370 ± 510	-	-	-
2510C	1.18	4.96 ± 1.05	2.64 ± 0.15	130 ± 410	-	-	-
2509	1.36	3.85 ± 0.68	2.63 ± 0.11	550 ± 270	-	-	-
River Usumacinta							
2514A	0.42	0.39 ± 0.09	4.55 ± 0.17	1920 ± 20	50	420	7.9 ± 1.1
2511	0.84	0.51 ± 0.10	3.65 ± 0.09	1870 ± 30	200	300	1.5 ± 0.1
2514B	1.14	1.17 ± 0.07	3.00 ± 0.08	1620 ± 30	-	-	-
2512	1.14	1.01 ± 0.07	3.00 ± 0.08	1670 ± 30	190	200	1.1 ± 0.1
2514C	1.34	1.56 ± 0.42	2.98 ± 0.11	1490 ± 140	-	-	-
2513	1.50	1.16 ± 0.08	2.95 ± 0.08	1620 ± 30	-	-	-

Table 5-1: Age estimates from full dating and profiling samples, together with sampled depths, and where possible sedimentation rates

6. References

Aitken, M.J., 1983, Dose rate data in SI units: PACT, v. 9, p. 69–76.

Bøtter-Jensen, L., Bulur, E., Duller, G.A.T., and Murray, A.S., 2000, Advances in luminescence instrument systems: Radiation Measurements, v. 32, p. 523-528.

Fuchs, M., and Lang, A., 2001, OSL dating of coarse-grain fluvial quartz using single-aliquot protocols on sediments from NE Peloponnese, Greece: Quaternary Science Reviews, v. 20, p. 783-787.

Lepper, K., Larsen, N.A., and McKeever, S.W.S., 2000, Equivalent dose distribution analysis of Holocene eolian and fluvial quartz sands from Central Oklahoma: Radiation Measurements, v. 32, p. 603-608.

Mejdahl, V., 1979, Thermoluminescence daing: Beta-dose attenuation in quartz grains Archaeometry, v. 21, p. 61-72.

Murray, A.S., and Wintle, A.G., 2000, Luminescence dating of quartz using an improved single-aliquot regenerative-dose protocol: Radiation Measurements, v. 32, p. 57-73.

NEA, 2000, The JEF-2.2 Nuclear Data Library: Nuclear Energy Agency, Organisation for economic Co-operation and Development. JEFF Report, v. 17.

Olley, J.M., Caitcheon, G.G., and Murray, A.S., 1998, The distribution of apparent dose as determined by optically stimulated luminescence in small aliquots of fluvial quartz: implications for dating young sediment: Quaternary Geochronology, v. 17, p. 1033-1040.

Olley, J.M., Caitcheon, G.G., and Roberts, R.G., 1999, The origin of dose distributions in fluvial sediments, and the prospect of dating single grains from fluvial deposits using optically stimulated luminescence: Radiation Measurements, v. 30, p. 207-217.

Prescott, J.R., and Hutton, J.T., 1994, Cosmic ray contributions to dose rates for luminescence and ESR dating: Large depths and long-term time variations: Radiation Measurements, v. 23, p. 497-500.

Sanderson, D.C.W., 1988, Thick source beta counting (TSBC): A rapid method for measuring beta dose-rates: International Journal of Radiation Applications and Instrumentation. Part D. Nuclear Tracks and Radiation Measurements, v. 14, p. 203-207.

Sanderson, D.C.W., and Murphy, S., 2010, Using simple portable OSL measurements and laboratory characterisation to help understand complex and heterogeneous sediment sequences for luminescence dating: Quaternary Geochronology, v. 5, p. 299-305.

Appendix A: Laboratory Profiling Results

A.1 SUTL2510/SUTL2514 Quartz

SUTL no.	Depth (cm)	Stored dose (Gy)		Sensitivity (counts/Gy)	
		Aliquot 1	Aliquot 2	Aliquot 1	Aliquot 2
2510A	0.18	5.99 ± 0.25	7.02 ± 1.00	1283 ± 20	309 ± 13
2510B	0.88	7.64 ± 1.97	5.03 ± 0.62	112 ± 10	244 ± 11
2510C	1.18	3.91 ± 0.57	6.01 ± 2.99	227 ± 11	66 ± 9
2514A	0.42	0.48 ± 0.06	0.30 ± 0.04	772 ± 16	1061 ± 18
2514B	1.14	1.24 ± 0.12	1.10 ± 0.11	565 ± 16	542 ± 14
2514C	1.34	1.14 ± 0.13	1.98 ± 0.13	423 ± 13	805 ± 17

A.2 SUTL2510/SUTL2514 Polymineral

SUTL no.	Depth (cm)	IRSL at 50°C		OSL at 125°C		TL to 500°C	
		Stored dose (Gy)	Sensitivity (photon counts/Gy)	Stored dose (Gy)	Sensitivity (photon counts/Gy)	Stored dose (Gy)	Sensitivity (photon counts/Gy)
2510A	0.18	16.7 ± 1	1448 ± 30	146.3 ± 8.7	1018 ± 26	244 ± 8.8	2225 ± 33
2510B	0.88	21.2 ± 2.4	462 ± 19	19.6 ± 1.3	735 ± 22	102.8 ± 5.3	1293 ± 25
2510C	1.18	28.8 ± 0.9	3878 ± 47	203.2 ± 9.3	2104 ± 37	284.5 ± 8.3	4086 ± 44
2514A	0.42	1.4 ± 0.1	1408 ± 30	5.3 ± 0.2	2429 ± 37	109.9 ± 4.9	1495 ± 27
2514B	1.14	4.1 ± 0.4	696 ± 22	12.4 ± 0.6	1342 ± 28	194.5 ± 11.3	986 ± 22
2514C	1.34	5.4 ± 0.3	1381 ± 29	20.1 ± 1	1798 ± 32	203.1 ± 9.4	1556 ± 27

Appendix B: Dose Response Curves

B.1 SUTL2508

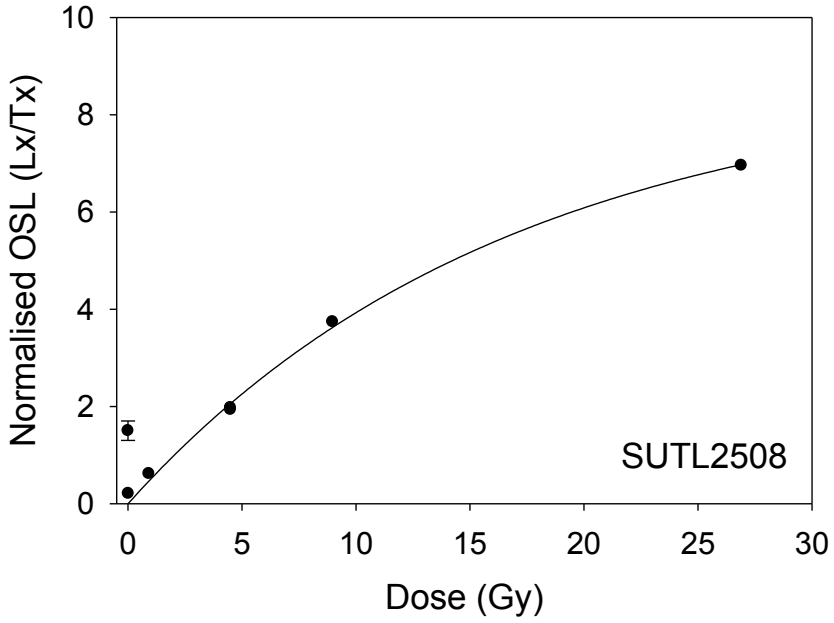

Composite dose response curve for sample SUTL2508. Lx = 0, 1, 5, 10, 30 and 5Gy; Tx = 2 Gy

B.2 SUTL2509

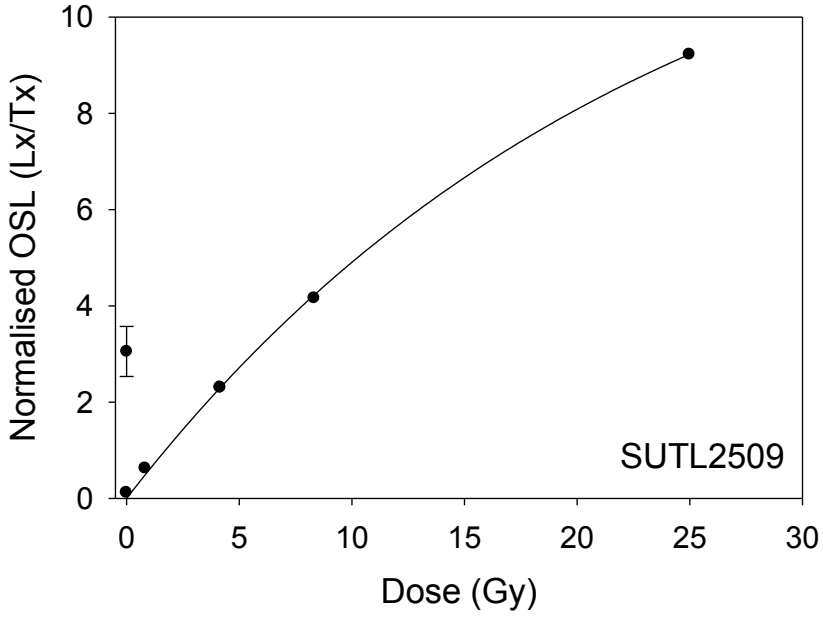

Composite dose response curve for sample SUTL2509. Lx = 0, 1, 5, 10, 30 and 5 Gy; Tx = 2 Gy

B.3 SUTL2511

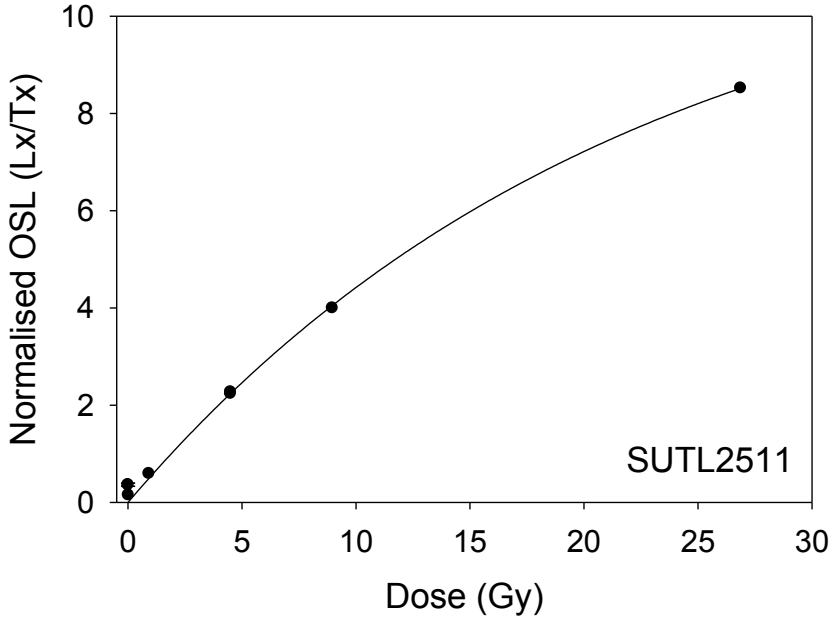

Composite dose response curve for sample SUTL2511. Lx = 0, 1, 5, 10, 30 and 5Gy; Tx = 2 Gy

B.4 SUTL2512

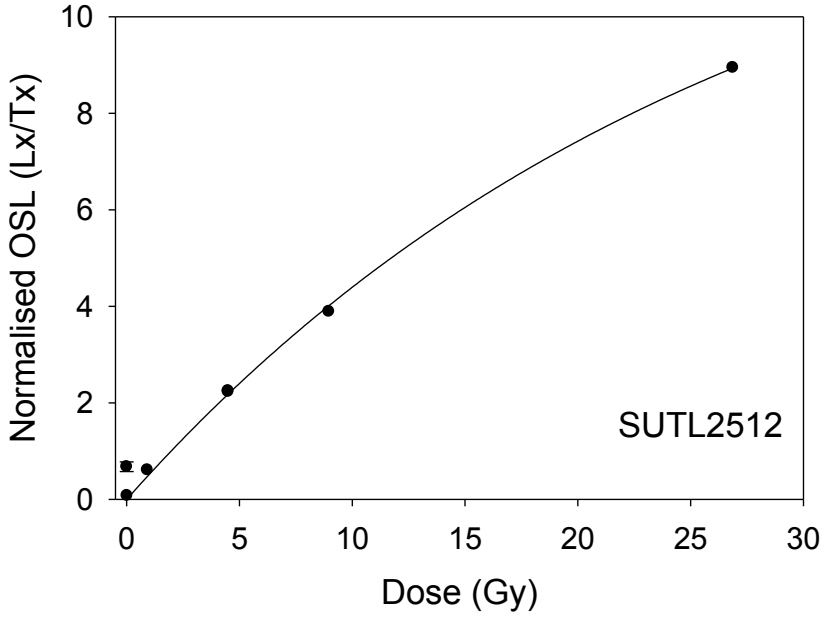

Composite dose response curve for sample SUTL2512. Lx = 0, 1, 5, 10, 30 and 5 Gy; Tx = 2 Gy

B.5 SUTL2513

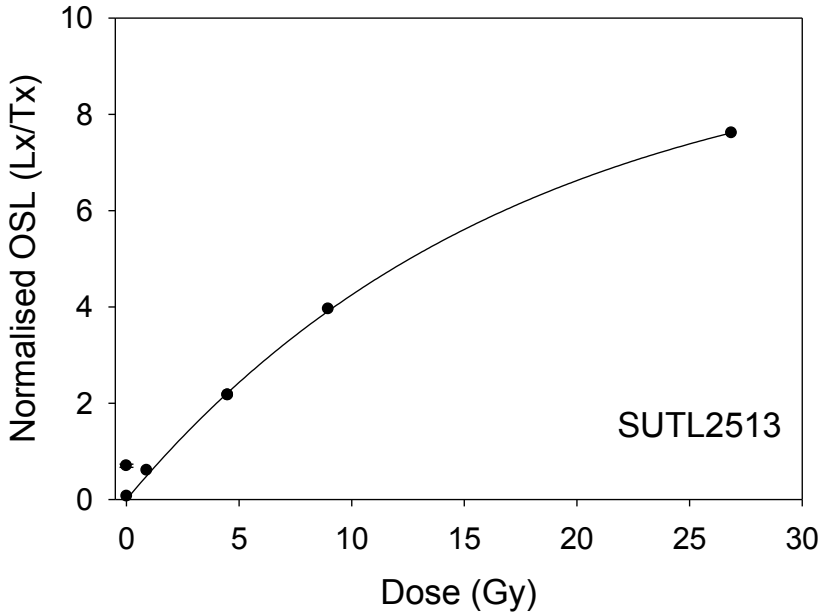

Composite dose response curve for sample SUTL2513. Lx = 0, 1, 5, 10, 30 and 5 Gy; Tx = 2 Gy

Appendix C: Radial plots

C.1 Radial plot for SUTL2508

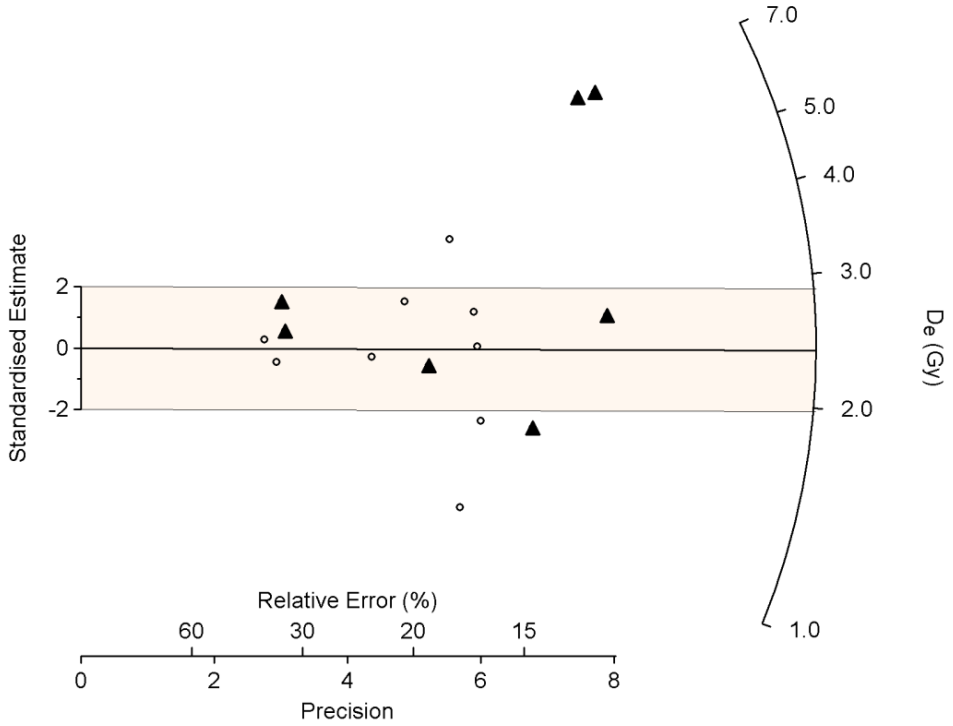

C.2 Radial plot for SUTL2509

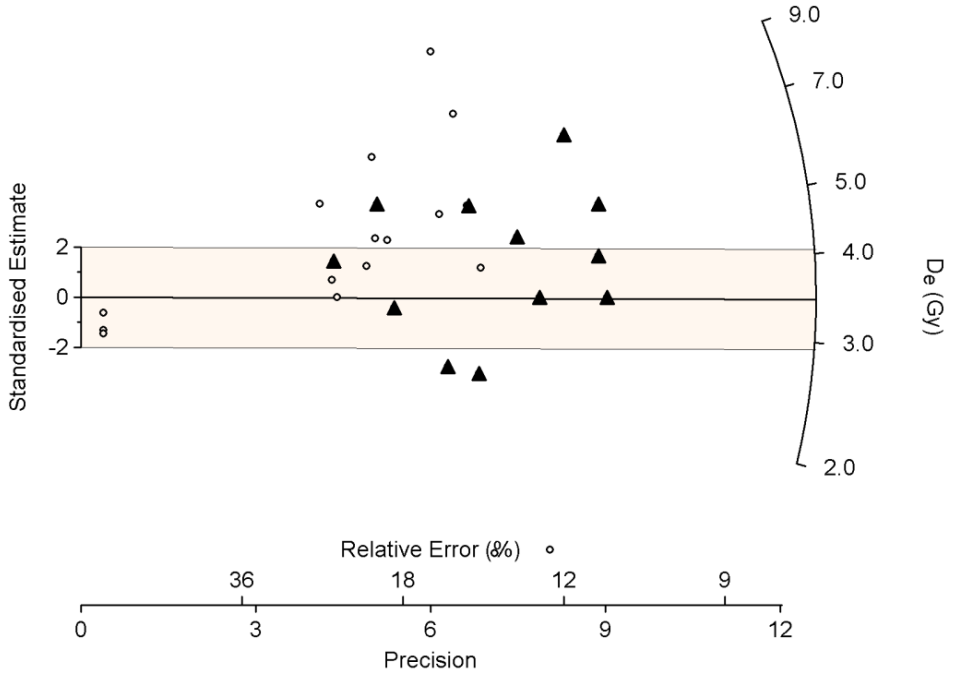

C.3 Radial plot for SUTL2511

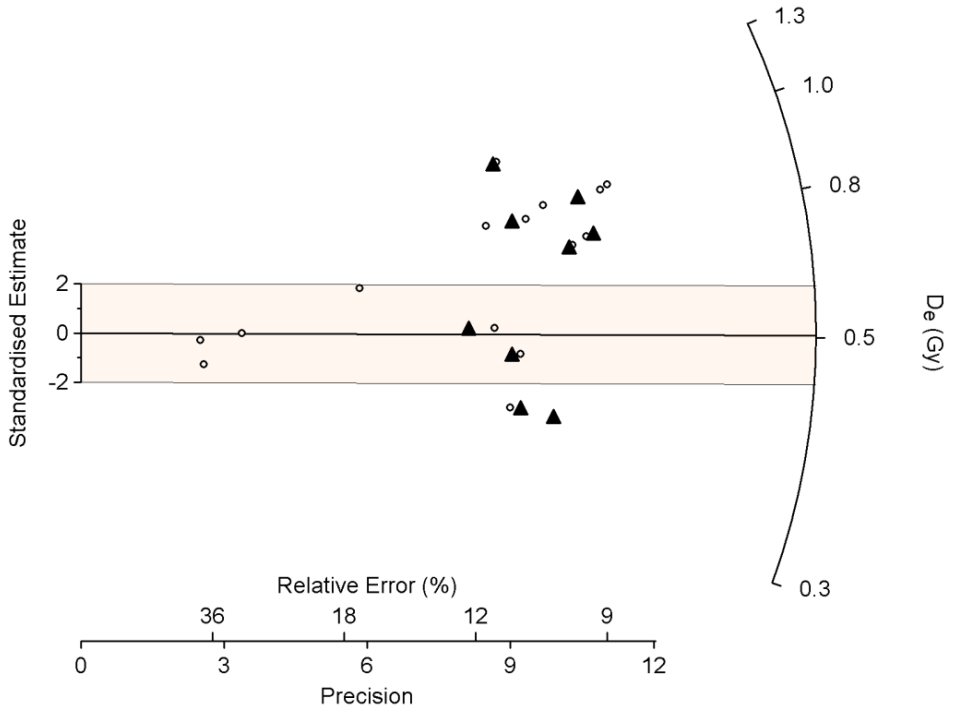

C.4 Radial plot for SUTL2512

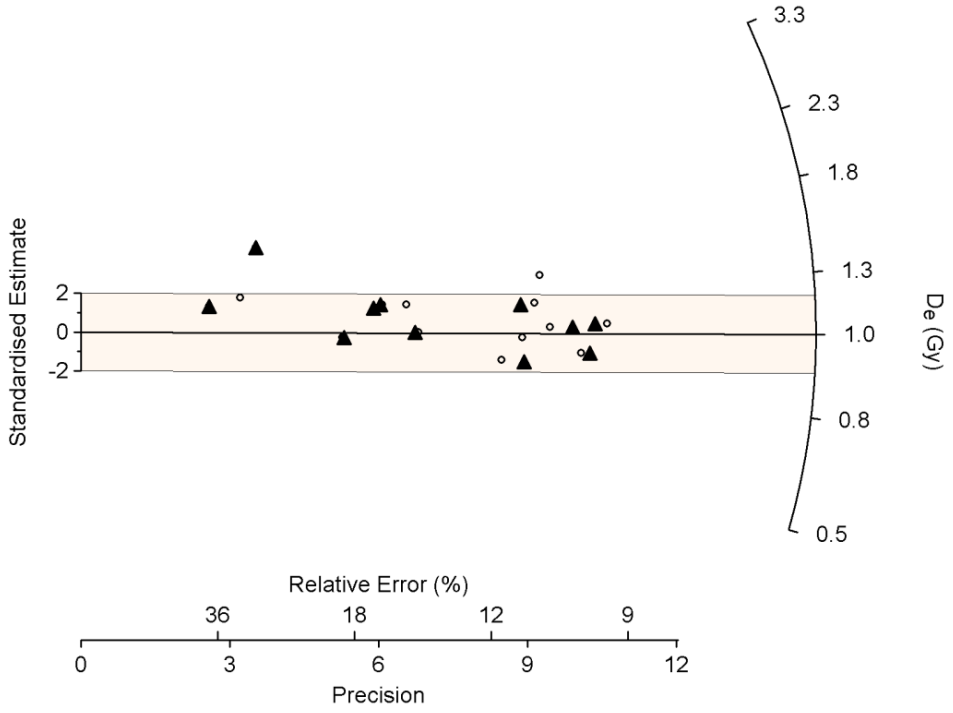

C.5 Radial plot for SUTL2513